Ligand Dynamics in the Solid: Lithium-fluorenide and Lithium-benzo[*b*]fluorenide *N*,*N*,*N*′,*N*′-Tetramethylethylenediamine (tmeda) Complexes[1])

by **Arnd Focke**[2]), **Heike Hausmann**[3]), **Steffen Jost**, and **Harald Günther***

Fakultät IV, OCII, University of Siegen, D-57068 Siegen (e-mail: guenmr@chemie.uni-siegen.de)

Dedicated with best wishes to *Dieter Seebach*, a pioneer of lithium NMR, on the occasion of his 75th birthday

The dynamic behavior of the *N*,*N*,*N*′,*N*′-tetramethylethylenediamine (tmeda) ligand has been studied in solid lithium-fluorenide(tmeda) (**3**) and lithium-benzo[*b*]fluorenide(tmeda) (**4**) using CP/MAS solid-state ^{13}C- and ^{15}N-NMR spectroscopy. It is shown that, in the ground state, the tmeda ligand is oriented parallel to the long molecular axis of the fluorenide and benzo[*b*]fluorenide systems. At low temperature (< 250 K), the ^{13}C-NMR spectrum exhibits two MeN signals. A dynamic process, assigned to a 180° rotation of the five-membered metallacycle (π-flip), leads at elevated temperatures to coalescence of these signals. Line-shape calculations yield $\Delta H^{\ddagger} = 42.7$ kJ mol^{-1}, $\Delta S^{\ddagger} = -5.3$ J mol^{-1} K^{-1}, and $\Delta G^{\ddagger}_{298} = 44.3$ kJ mol^{-1} for **3**, and $\Delta H^{\ddagger} = 36.8$ kJ mol^{-1}, $\Delta S^{\ddagger} = -17.7$ J mol^{-1} K^{-1}, and $\Delta G^{\ddagger}_{298} = 42.1$ kJ mol^{-1} for **4**, respectively. A second dynamic process, assigned to ring inversion of the tmeda ligand, was detected from the temperature dependence of $T_{1\rho}$, the ^{13}C spin-lattice relaxation time in the rotating frame, and led to $\Delta H^{\ddagger} = 24.8$ kJ mol^{-1}, $\Delta S^{\ddagger} = -49.2$ J mol^{-1} K^{-1}, and $\Delta G^{\ddagger}_{298} = 39.5$ kJ mol^{-1} for **3**, and $\Delta H^{\ddagger} = 18.2$ kJ mol^{-1}, $\Delta S^{\ddagger} = -65.3$ J mol^{-1} K^{-1}, and $\Delta G^{\ddagger}_{298} = 37.7$ kJ mol^{-1} for **4**, respectively. For (D_{12})-**3**, the rotation of the CD_3 groups has also been studied, and a barrier E_a of 14.1 kJ mol^{-1} was found.

Introduction. – Aggregation and complex formation with donor ligands are typical properties of organolithium compounds that are well-known from NMR investigations in solution [2] and X-ray structural analyses of crystalline solids [3]. In addition, many NMR studies have revealed the existence of *intra*- and *inter*-aggregate dynamic processes where coordinative bonds between donor ligands and Li-atoms are cleaved and re-formed [4]. These processes are also important for the reactivity of these systems that are widely used in organic synthesis. The determination of the energy barriers involved is thus of general interest. However, in solution, where cleavage of donor bonds can occur, it is often difficult to distinguish between various forms of ligand mobility or to decide between *intra*- and *inter*-aggregate processes, because the barriers involved are of similar magnitude [5]. For a heterocyclic five-membered ring, for example, that is formed by *N*,*N*,*N*′,*N*′-tetramethylethylenediamine (tmeda) coordination to Li, conceivable *intra*-molecular dynamic processes are rotation or ring inversion as shown in the *Scheme*.

---

1) NMR Spectroscopy of Organolithium Compounds, Part XXVIII; for Part XXVII see [1].

2) Deceased October 29, 1997.

3) Present address: Institute of Organic Chemistry, University of Giessen (e-mail: heike.hausmann@org.chemie.uni-giessen.de).

Scheme

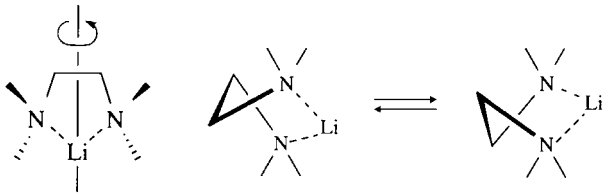

In solution, both processes can be formulated with and without cleavage of the chelate bonds.

Ligand mobility can also be assumed for solid organolithium compounds on the basis of the large thermal vibrational ellipsoids observed by X-ray structure determinations of many of these systems [3]. In the solid, mechanisms with bond cleavage as well as the occurrence of *inter*-aggregate processes can be excluded. It is thus expected that dynamic reorientations are limited to a rotation process of the whole molecule and to *intra*-molecular conformational changes. Both can be readily characterized by solid-state NMR spectroscopy – also a valuable tool for investigations of organolithium compounds [6] – through relaxation-time measurements and line-shape changes [7]. As far as conformational dynamics are concerned, because of the different steric requirements, we can expect that, for example, the energy barrier for ring inversion on one side and the 180° ring flip on the other differs.

Earlier, we reported on the mobility of tmeda ligands in phenyllithium$_2$(tmeda)$_2$ (**1**) and *trans*-dilithionaphthalinediide(tmeda)$_2$ (**2**) [8]. For the process assigned to ring inversion of the five-membered metallacycle, a barrier $\Delta G^{\ddagger}$ of *ca.* 40 kJ mol^{-1} was found, and for the 180° rotation (π-flip) we measured *ca.* 65 kJ mol^{-1}. We now investigated the dynamic behavior of the tmeda ligands in solid lithium-fluorenide-(tmeda) (**3**) and lithium-benzo[*b*]fluorenide(tmeda) (**4**) using CP/MAS solid-state ^{13}C-NMR and, for **3**, ^{15}N-NMR spectroscopy. The line shapes of these spectra are sensitive to dynamic processes with rate constants k between 10^2 and 10^5, while measurements of the temperature-dependent spin lattice relaxation time in the rotating frame, $T_{1\rho}$, extends this range to 10^4 – 10^7. Line-shape analysis follows the procedures well-known from solution studies [9], and the use of $T_{1\rho}$ measurements has been described in detail by *Riddell* [10].

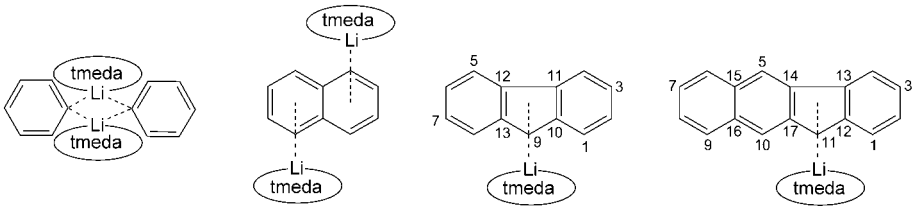

1 **2** **3** **4**

TMEDA = $Me_2NCH_2CH_2NMe_2$

For both systems, **3** and **4**, three *intra*-molecular conformational processes may be expected (*Fig. 1*):

i) 180° Rotation (π-flip) of the Li-tmeda metallacycle (**A** $\rightleftharpoons$ **B**), with an exchange of the Me groups of the back side above C(4,5) with those of the front side above C(1,8) (1 $\rightleftharpoons$ 3 and 2 $\rightleftharpoons$ 4) and an exchange of the CH_2 groups,
ii) Ring inversion in this unit (**C** $\rightleftharpoons$ **D**) that exchanges the CH_2 groups, and
iii) Me-group rotation.

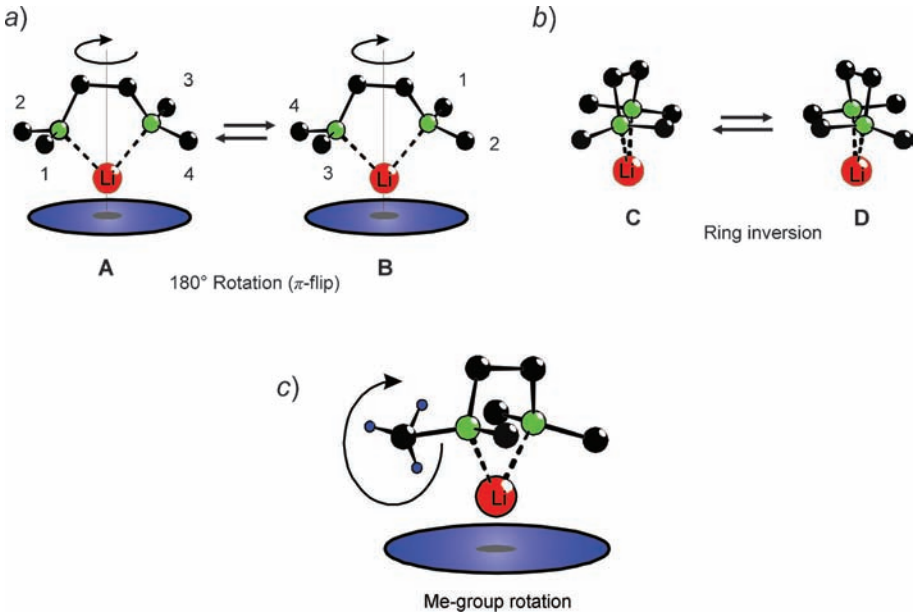

Fig. 1. *Expected dynamic processes for solid* **3** *and* **4***:* a) *rotation of the tmeda ligand;* b) *ring inversion of the tmeda ligand;* c) *rotation of the Me group*

Results. – *The Solid-State Structures of* **3** *and* **4**. To have a firm basis for the interpretation of the NMR results, knowledge of the solid-state structures of **3** and **4** was important. X-Ray results are available for **3** [11] but not for **4**. Structures of both systems were thus calculated using the *ab initio Hartree–Fock* method with a 3-21G(*) basis set. The results, displayed in *Fig. 2*, show for **3** excellent agreement with the X-ray data and the results of a REDOR study [12] that lends support also for the structure of **4**. Both systems, prepared in hexane or benzene by reaction of fluorene or benzo[*b*]fluorene, respecively, with BuLi in the presence of equimolecular amounts of TMEDA, were calculated as contact ion pairs, in agreement with their ^{7}Li quadrupolar coupling constant, $\chi(^7\text{Li})$, and their ^{7}Li chemical shift, $\delta(^7\text{Li})$. For **3**, *Johnels et al.* reported $\chi(^7\text{Li}) = 179$ kHz and $\delta(^7\text{Li}) = -7.5$ ppm (rel. to LiCl/H_2O) [13], and for **4** we found $\chi(^7\text{Li}) = 192$ kHz at 196 K and $\delta(^7\text{Li}) = -6.94$ ppm at 293 K. The shielding observed for ^{7}Li is a consequence of the position of the Li^+ cation above the diatropic five-membered ring [3b,c], and the quadrupole coupling constant of ^{7}Li was earlier identified as an indicator for the solid-state structure with values >100 kHz typical for contact ion pairs [14]. Interestingly, for **4** $\chi(^7\text{Li})$ was only 12–16 kHz at room temperature and increased by lowering the temperature to the value given above with 120 kHz at 209.6 K. This behavior can be attributed to the high-temperature

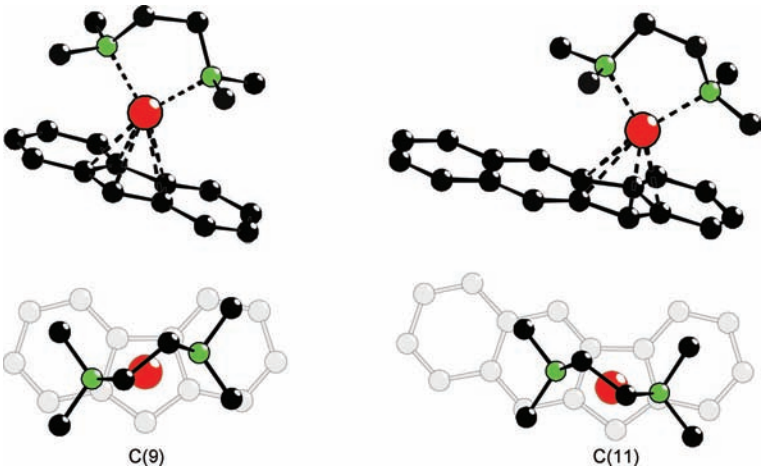

Fig. 2. *Calculated structures for* **3** (*left*) *and* **4** (*right*)

conformational mobility of the five-membered Li–tmeda ring. A similar temperature dependence of $\chi(^7Li)$ was found for **1** [8].

Solid-State ^{13}C-NMR Spectra of **3** *and* **4**. The room-temperature 75-MHz ^{13}C CP/MAS solid-state NMR spectra of both complexes are shown in *Figs. 3* and *4*, respectively. The spectrum of **3** (*Fig. 3*, *a*) shows the signals of the sp^2-hybridized C-atoms between 78.8 and 134.2 ppm as well as a *singlet* for the tmeda Me resonance at 44.1 ppm. The assignment is based on the results of the solution spectrum with a two-dimensional $^{13}C,^1H$ correlation. For this purpose, the ^1H-assignment was derived by COSY spectroscopy and a NOE difference spectrum that documents the spatial proximity of H–C(1) and H–C(9). The signal of the tmeda CH_2 groups is strongly broadened at room temperature (dipolar broadening, see below) and appears from the noise at lower temperatures. At 226 K, it is found at 54.4 ppm. The results are collected in *Table 1*.

Table 1. *^{13}C Chemical Shifts* [ppm] *of* **3** *in the Solid* (*a* and *b*) *and in Solution* (*c*)

Entry	C(10,13)	C(2,7,4,5)	C(1,8,11,12)	C(3,6)	C(9)	MeN	CH_2	*T* [K]
a	134.2	122.9	118.4	114.0	78.8	44.1	54.4[a])	289
b[b])	134	122	119	114	78			
c	137.8	119.0, 118.8	116.3, 123.1	108.0	82.4	45.9	58.9	293

[a]) At 226 K; 55.9 ppm at 343 K. [b]) REDOR Study [12].

For **4**, the signals of the sp^2 C-atoms are closely spaced between 118 and 135 ppm with the resonance of C(11) at 78.4 ppm, and the signal of the tmeda Me group is found at 44.2 ppm (*Fig. 4*,*a*). The signal of the tmeda CH_2 groups is again strongly broadened at room temperature and is found at 260 K at 54.9 ppm. The six resonances of the quarternary C-atoms were separately detected by a $^{13}C\{^1H\}$-SELTICS spectrum [15] (*Fig. 4*,*b*). Further assignments of the ^{13}C resonances were not attempted. In both

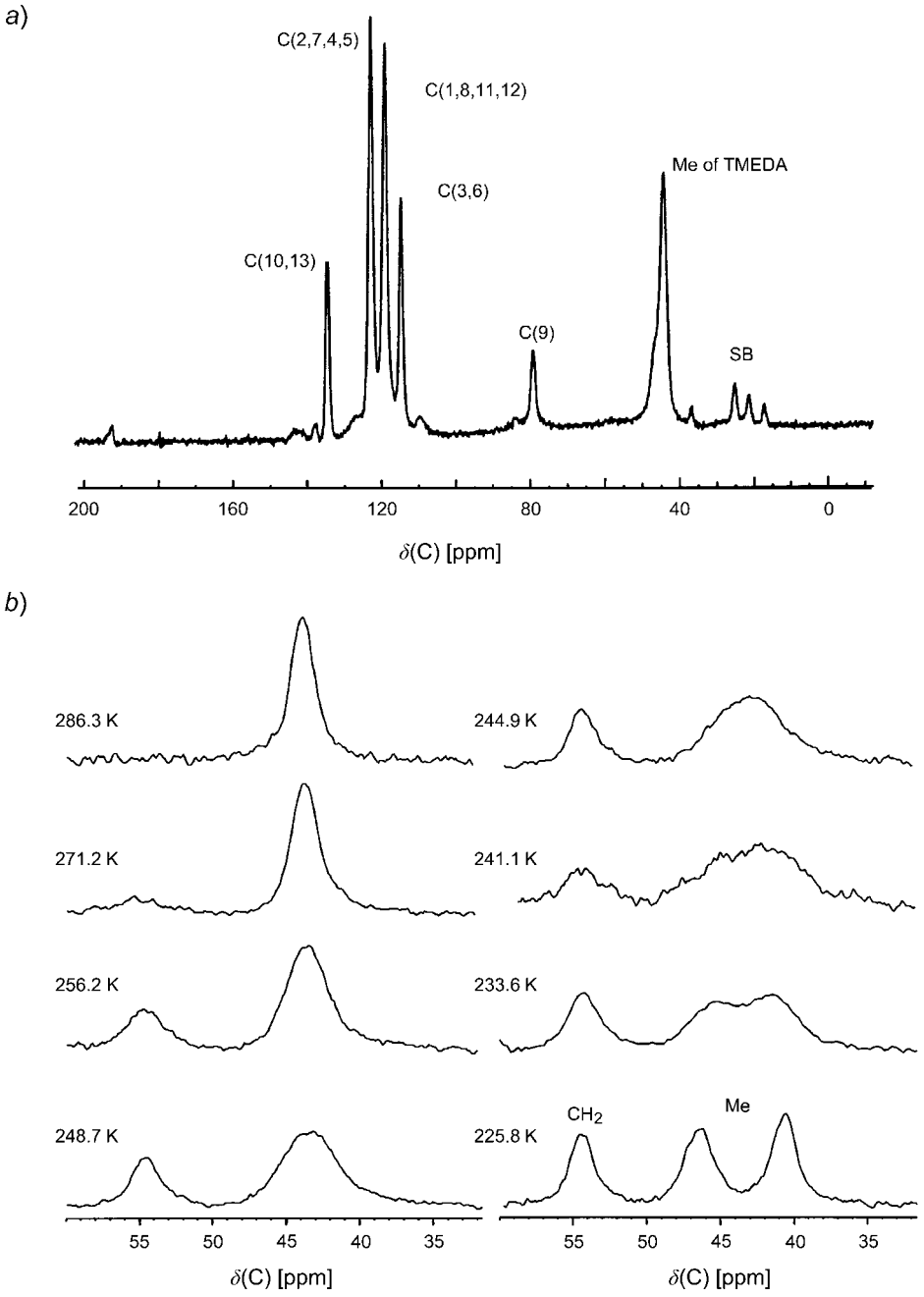

Fig. 3. *75-MHz CP/MAS ^{13}C-NMR Spectrum of* **3** *at room temperature* (*a*) *and partial spectra at variable temperature* (*b*). SB = Sideband

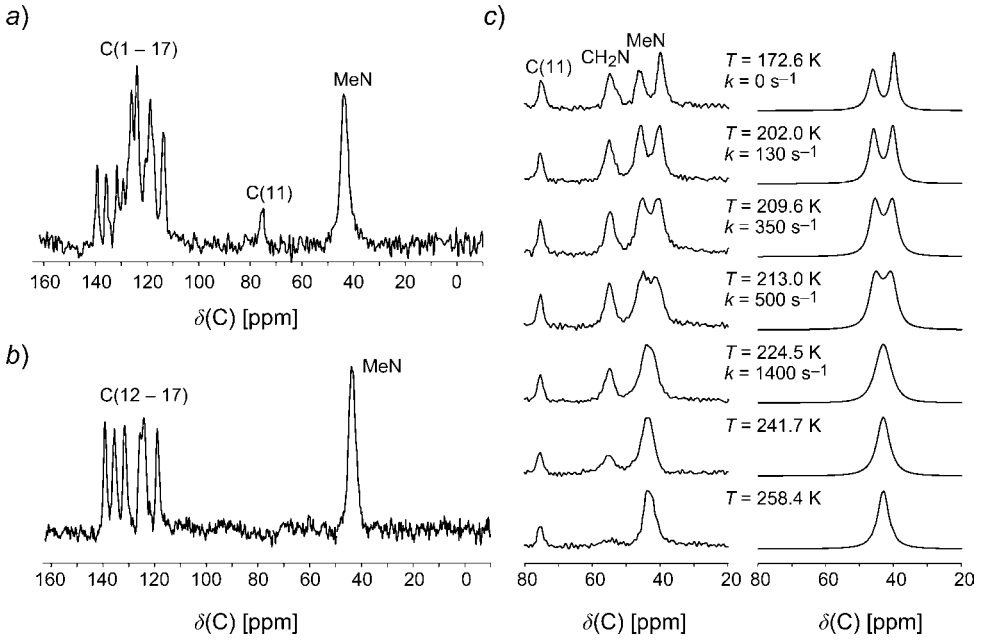

Fig. 4. a) *75-MHz CP/MAS* ^{13}*C-NMR Spectrum of* **4** *at room temperature*, b) *CP-MAS SELTICS spectrum*, *and* c) *temperature-dependent Me resonance region* (left) *with calculated spectra* (right)

spectra, signals of the tmeda CH_2 C-atoms are not detected at or near room temperature because of dipolar broadening [16] (see below).

The 25-MHz ^{13}C CP/MAS solid-state NMR spectrum of **3** had already shown the temperature dependence of the tmeda ^{13}C signals at 44 ppm [17], but no detailed analysis was attempted. At 75 MHz, we found broadening of the tmeda Me signal at 290 K which finally splits at 234 K into two separate *singlet*s (*Fig. 3*,*b*). At *ca.* 275 K, the signal of the tmeda CH_2 resonance that is not detected at room temperature, presumably due to the effect of dipolar broadening, starts to appear from the noise. Actually, for a π-flip a line splitting would also be expected for the ^{13}C signal of the CH_2 groups (compare their position in the structure shown in *Fig. 2*), but the large line width apparently prevents a line separation. The participation of the CH_2 resonance on a dynamic process is, however, documented by the phenomenon of dipolar broadening [16] of their resonance at elevated temperatures that results for chemical exchange of signals from the increased transverse relaxation in a situation where the power of the proton decoupler field matches the exchange rate k between non-equivalent positions. At the point of largest line width, the condition $\gamma B_2 = k$ holds. Through NMR line-shape analysis for an exchange process of the Me signals between two equally populated sites [18] in the temperature range between 202 and 248 K, the rate constants k for a reversible first order process were obtained (see *Table 2*).

Similar line-shape changes are observed for the spectrum of **4** again with dipolar broadening for the CH_2 resonance. Experimental and calculated exchange spectra

Table 2. *First-Order Rate Constants* k [s^{-1}] *for the Reorientation of the tmeda Ligand in* **3** *and* **4**

3	T [K]	201.7	208.8	212.4	215.9	219.5	223.0	226.6	230.2	233.7	237.3	240.8	247.9
	k [s^{-1}]	18	45	70	110	170	260	375	526	700	1000	1400	2500
4	T [K]	202.0	206.2	209.6	213.0	214.6	216.3	218.0	219.7	224.5			
	k [s^{-1}]	130	270	350	500	650	735	850	870	1400			

between 172 and 258 K, based, as mentioned above, on an exchange process between two equally populated sites, are shown in *Fig. 4*, *c*, and the rate constants k are compiled in *Table 2*. Finally, from the *Eyring* and *Arrhenius* diagrams of the exchange processes we derived the kinetic data collected in *Table 3* that shows also the statistical errors.

Through the measurement of $T_{1\rho}$, the spin lattice relaxation time, in the rotating frame, and an analysis that followed the method described by *Riddell* [10] it was possible to extend the investigations to a larger temperature range (*Fig. 5*). $T_{1\rho}$ is sensitive for internal molecular mobility with a frequency similar to the spin lock frequency of the CP experiment. $T_{1\rho}$ is temperature-dependent, because the rate for molecular motion, characterized by the rotational correlation time, τ_c, changes with temperature. At a temperature where, for the strength of the ^{13}C spin lock field, ω_1, the condition $\omega_1\tau_c = 1$ holds, $T_{1\rho}$ will have a minimum. For **3**, well-defined $T_{1\rho}$ minima were found for the signals at 44 and 122 ppm ($^{13}CH_3N$ and $^{13}C(2,7)$). For **4**, the $^{13}CH_3N$ was selected for the $T_{1\rho}$ measurements where we used the standard CP-MAS sequence complemented by a variable relaxation delay τ between spin lock and detection.

For the dipolar relaxation between unlike spins, we have *Eqn. 1:*

$$\frac{1}{T_{1\rho}} = \frac{B^2\tau_c}{1+\omega_1^2\tau_c^2} \tag{1}$$

that relates $T_{1\rho}$ and ω_1 with B^2 as a measure of the dipolar interaction strength between ^{13}C and ^{1}H in the rotating frame. For the minimum ($\omega_1\tau_c = 1$), we have from *Eqn. 1*:

$$B^2 = \frac{2}{\tau_c^{\min} \times T_{1\rho}^{\min}} \tag{2}$$

$$\text{and with } \tau_c^{\min} = \frac{1}{\omega_1}, \text{ it follows } B^2 = \frac{2\,\omega_1}{T_{1\rho}^{\min}} \tag{3}$$

The minima of the $T_{1\rho}/T$ curves (*Fig. 5*) were determined by non-linear curve fitting and allowed calculation of B^2 *via Eqn. 2* with ω_1 obtained from the CP pulse length t_p by $\omega_1 = \pi/2\,t_p$. It was then possible to solve *Eqn. 1* for τ_c, and calculate the rate constants k by $k = 2/\tau_c$ from the measured $T_{1\rho}$ values and the known quantities of B^2 and ω_1. The factor 2 was introduced for the dynamic process assigned to ring inversion, because *two* inversions are necessary in order that the ring atoms return to their original positions. The kinetic parameters derived from these measurements are also given in *Table 3*.

A simple check for $\Delta G^{\ddagger}$ obtained from the line-shape calculations for the π-flip is possible with the well-known equation $k_{\text{coalesc.}} = 2.22 \times \Delta\nu$ [19]. This gives with the data of *Table 4* $k = 980$ and 1043 s^{-1} for **3** and **4**, respectively. Coalescence temperatures T_c

Table 3. *Kinetic Data for Dynamic Processes in* **3** *and* **4**

	From line-shape changes (π-flip $\mathbf{A} \rightleftharpoons \mathbf{B}$)[a]		From $T_{1\rho}$ measurements (ring inversion $\mathbf{C} \rightleftharpoons \mathbf{D}$)[b]			Me Rotation
	3	**4**	**3**[a])	**3**[b])	**4**	(D_{12})-**3**
$\Delta H^{\ddagger}$ [kJ mol^{-1}]	42.72 ± 0.47[c])	36.80 ± 1.91	24.84 ± 0.71	24.15 ± 0.96	18.24 ± 0.85	12.90 ± 0.52
$\Delta S^{\ddagger}$ [J mol^{-1} K^{-1}]	− 5.3 ± 2.08	− 17.70 ± 8.96	− 49.20 ± 2.40	− 47.32 ± 3.24	− 65.32 ± 3.10	− 31.8 ± 3.5
$\Delta G^{\ddagger}_{298}$ [kJ mol^{-1}]	44.31	42.07	39.50	38.25	37.71	22.38
E_a	44.57 ± 0.45	38.61 ± 1.89	27.26 ± 0.72	26.58 ± 0.99	20.48 ± 0.89	14.13 ± 0.51
ln A	29.53 ± 0.24	28.02 ± 1.07	24.51 ± 0.39	24.75 ± 0.40	22.51 ± 0.35	25.93 ± 0.42
Temp. range ΔT [K]	46	22	68	92	107	51
Number of data points, correlation coefficient	12, r = 0.999	9, r = 0.99	9, r = 0.99	14, r = 0.99	18, r = 0.98	7, r = 0.99

[a]) Signal at 122.9 ppm. [b]) Signal at 44.1 ppm. [c]) Statistical error.

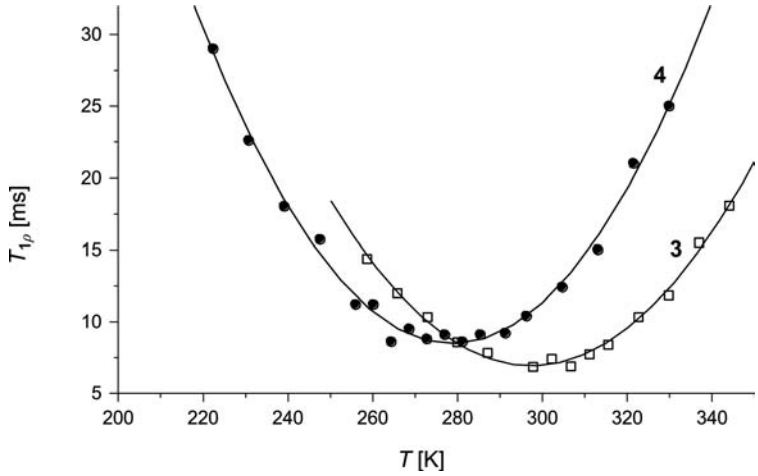

Fig. 5. $T_{1\rho}$/T *Curves for* **3** (signal at 122 ppm) *and* **4**

of 235 and 215 K estimated from the spectra shown in *Figs. 3* and *4*, and the *Eyring* equation $\Delta G^{\ddagger} = RT_c[22.96 + \ln(T_c/\Delta\nu)]$ yield $\Delta G^{\ddagger}_{235} = 43.6$ and $\Delta G^{\ddagger}_{215} = 39.6$ kJ mol^{-1} for **3** and **4**, respectively, in good agreement with the data of *Table 3*. Another prediction for $\Delta G^{\ddagger}$ of **3** is possible from the dipolar broadening of the CH_2 resonance that can be estimated from the spectra shown in *Fig. 3,b*, to appear at *ca.* 290 K. With $k = 5.2 \times 10^5$ s^{-1} (*Table 4*) from $\gamma B_2 = \omega_1$ and the *Eyring* equation $\Delta G^{\ddagger} = RT$ [23.76 – $\ln(k/T)$], we obtain $\Delta G^{\ddagger}_{290} = 39.2$ kJ mol^{-1}. This agrees well with $\Delta G^{\ddagger}_{298}$ found for the ring inversion in **3** (*Table 3*). A similar estimate for **4** with *ca.* 260 K and $k = 3.9 \times 10^5$ s^{-1} from *Table 4* yields $\Delta G^{\ddagger}_{260} = 35.5$ kJ mol^{-1}.

Table 4. *Experimental Data of the Line-Shape Calculations and* $T_{1\rho}$ *Measurements for* **3** *and* **4**

	3	**4**
Line-shape calculations		
Chemical shift $\Delta\nu$ [Hz]	441	470
Natural line width Δ [Hz]	112 (C(10))	235
$T_{1\rho}$ Measurements		
Pulse width t_p [μs]	3	4
ω_1 [s^{-1}]	5.2×10^5	3.9×10^5
$\tau_c^{\min}$ [μs]	1.9	2.8
$T_{1\rho}^{\min}$ [ms]	6.8	8.8
Dipolar interaction B^2 [s^{-2}]	15.3×10^7	8.9×10^7

Discussion. – From the two dynamic processes described for **3** and **4**, we assign that associated with the line-shape changes to the 180° rotation of the tmeda ring. According to the structure of both systems, this π-flip is compatible with the exchange of the Me groups between positions *cis* and *trans* to C(9) or C(11), respectively, as indicated by the equilibrium $\mathbf{A} \rightleftharpoons \mathbf{B}$ (*Fig. 1*). The orthogonal orientation of the tmeda

ligand, parallel to the short axis of the fluorenide ligand, would not be compatible with the NMR results, because the ^{15}N signal of **3** ($\delta = -360.8$ ppm relative to external $MeNO_3$ at 219 K) shows no splitting over the whole temperature region, and ^{15}N is thus exchanged between equivalent positions.

The $\Delta G^{\ddagger}_{298}$ values for **3** and **4** are smaller by *ca.* 20 kJ mol^{-1} than those found for the same process in **1** and **2** [8]. This may be considered as the result of the negative activation entropy, because the activation enthalpies $\Delta H^{\ddagger}$ are comparable with the value found for **1** (48.8 kJ mol^{-1}). For **1**, we had observed a positive $\Delta S^{\ddagger}$ of 28 J mol^{-1} K^{-1}. This difference may originate from packing forces in the crystals that influence the entropy of the transition state differently. Of course, entropy data from DNMR recordings are always somewhat problematic, especially if the temperature range is small, and the spectral line shape is of lower quality than that obtained in solution DNMR experiments, a consequence of the CP/MAS solid-state spectra. Nevertheless, the sign change for $\Delta S^{\ddagger}$ seems to be a reliable indicator of the different situation for the reorientation of the tmeda unit in complex **1** on one side, and in **3** and **4** on the other.

The second dynamic process is then due to the inversion of the tmeda ring in **3** and **4** (**C** $\rightleftharpoons$ **D** in *Fig. 1*). The alternative, a rotational movement of the whole molecule seems less likely, since the data for **3** and **4** are comparable. On the basis of the different size of both complexes, larger differences in the kinetic data would be expected. The $\Delta G^{\ddagger}$ values found are close to those measured earlier for **1** (40 kJ mol^{-1}) [8], and the activation enthalpy $\Delta H^{\ddagger}$ as well as the *Arrhenius* barrier E_a are not unexpected smaller by *ca.* 20 kJ mol^{-1} than that found for the π-flip described above. For **4** at *ca.* 220 K, the rate constant of the ring inversion is larger by a factor of 130 than that of the π-flip. The large negative activation entropies point to a considerable loss of vibrational motions in the transition state that is not surprising if one assumes a planar structure with increased ring strain.

It is interesting to compare our data with those reported by *Cabral* and *Fraenkel* [5a] for the π-flip of the tmeda ligand in tetramethylallyllithium(tmeda) in (D_{10})diethyl ether *solution*. They found $\Delta H^{\ddagger} = 32.6$ kJ mol^{-1} and $\Delta S^{\ddagger} = -22$ J mol^{-1} K^{-1} that yields $\Delta G^{\ddagger}_{298} = 39.2$ kJ mol^{-1}, in good agreement with our data for **3** and **4**. In solution, a second process, the dissociation of the ion pair, was observed and characterized. Later, 29 kJ mol^{-1} and -50 J mol^{-1} K^{-1} for $\Delta H^{\ddagger}$ and $\Delta S^{\ddagger}$, respectively, were reported for the reorientation of the coordinated tmeda ligand on one side of the allyl plane, presumably a π-flip, in a variety of allyl-lithium compounds [20]. For the π-flip, $\Delta H^{\ddagger}$ is smaller than in the solid, and the difference may be seen as that between solvation effects in solution and packing forces in the solid. Theoretical calculations for the barriers of the dynamic processes in the tmeda complex of *exo*,*exo*-[1,3-bis(trimethylsilyl)allyl]lithium [5b] (π-flip, MNDO, 39 kJ mol^{-1}; ring inversion, *ab initio*, 29 kJ mol^{-1}) compare very well with our data for $\Delta H^{\ddagger}$ or E_a of **3** and **4**.

Finally, it was of interest to measure the barrier for the Me-group rotation, the third dynamic process expected. For this purpose, we used **3** with deuterated Me groups and recorded variable-temperature ^2H-NMR spectra by the quadrupolar-echo technique [21]. The sensitivity of ^2H-NMR line shapes in static solid-state spectra is well-known and documented [22]. As *Fig. 6* demonstrates, typical line-shape changes were observed that were analyzed by spectral simulation. The *Arrhenius* activation barrier E_a of 14.1 kJ mol^{-1} determined in (D_{12})-**3** is only slightly higher than barriers found in

the gas phase for internal rotation in ethane (12.11 kJ mol^{-1} [23]) or $MeNH_2$ (8.2 kJ mol^{-1} [24]). A considerable increase compared to our $\Delta H^{\ddagger}$ value for Me rotation is not unexpectedly found for ^{t}Bu rotation in the solid, where *Riddell* reported 38.2 and 33.5 kJ mol^{-1} for *cis*-4-(*tert*-butyl)-1-[(*tert*-butylsulfonyl)]cyclohexane [10b] and 26.3 and 31.8 kJ mol^{-1} for *cis*-2-(*tert*-butyl)-5-[(*tert*-butyl)sulfonyl]-1,3-dioxane [25].

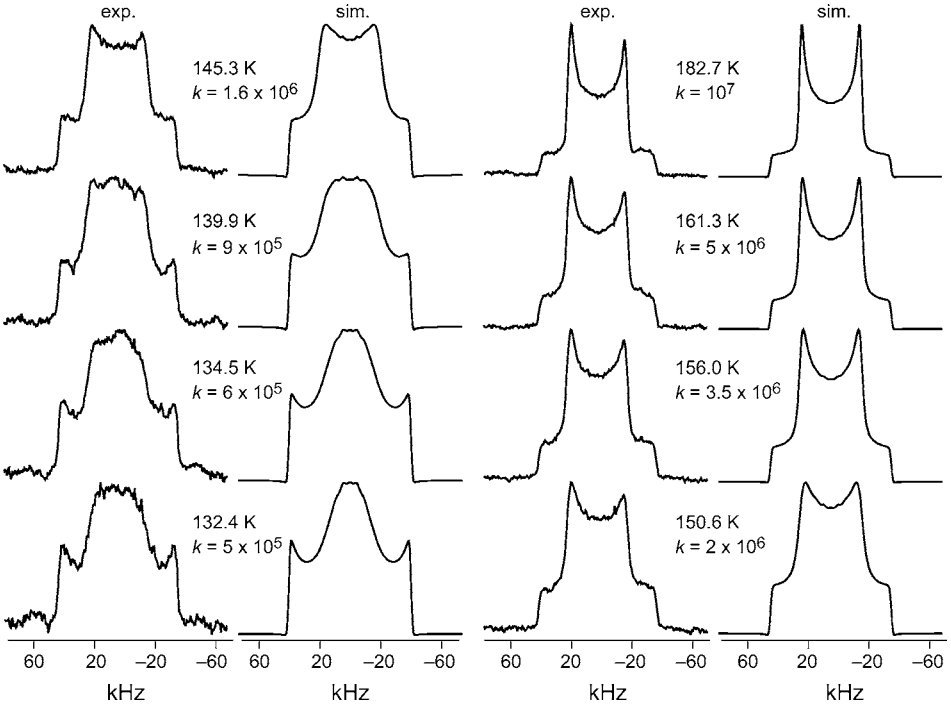

Fig. 6. *Experimental and simulated static deuterium quadrupolar-echo solid-state spectra of* (D_{12})-**3**. Rate constants k in s^{-1}.

We are indebted to the late Prof. *R. R. Vold* for supplying us with the *Program MXET1* and to the *Volkswagen-Stiftung* for a spectrometer grant.

Experimental Part

General. For the synthesis of **3** and **4**, the freshly sublimed samples (2 – 3 mmol) of the hydrocarbons (*Fluka*) were suspended under Ar in hexane; TMEDA (4.0 mmol) and a soln. of BuLi (5.0 mmol) in hexane (1.6M) were added, and the deep-red mixture was stirred overnight. The solvent was removed with a pipette, and the precipitate was washed three times with hexane and dried under vacuum to yield *ca.* 0.5 g of fine-crystalline material which was later transferred into the NMR rotor, again under Ar. To remove traces of H_2O, the rotors were heated before and dried under vacuum. For the synthesis of (D_{12})-**3**, (D_{12})TMEDA was obtained from *Fluka*.

Spectra. Solid-state ^{13}C CP/MAS NMR spectra were recorded with a *Bruker MSL 300* spectrometer and 4-mm ZrO_2 rotors with Kel-F caps; the rotational frequency, 4 kHz; sweep width, 20 kHz; CP contact

Table 5. *$T_{1\rho}$ Data* ([ms]) *and First-Order Rate Constants k* ([s^{-1}]) *for the Ring Inversion of the tmeda Ligand in* **3** *and* **4**

3	T [K][a]	270.0	274.3	278.5	287.0	291.2	295.4	303.9	312.3	320.8	329.2	337.7							
	$T_{1\rho}$ [ms][a])	54.6	45.7	42.2	36.6	30.2	30.4	33.6	36.4	44.8	55.6	60.2							
	k [10^5 s^{-1}][a])	2.36	2.98	3.36	4.33	9.53	–	–	11.83	16.89	22.46	24.72							
3	T [K]	251.5	258.6	265.7	272.9	280.0	287.1	297.8	302.2	306.7	311.1	315.6	322.7	329.8	336.9	344.0			
	$T_{1\rho}$ [ms][b])	16.3	14.8	12.3	10.4	8.6	7.7	6.7	7.1	7.5	8.2	8.7	10.6	11.9	16.3	20.0			
	k [10^5 s^{-1}][b])	2.30	2.56	3.17	3.92	5.17	6.36	–	13.86	16.25	19.53	21.60	28.68	33.18	47.68	59.58			
4	T [K]	222.4	230.8	239.2	247.6	256.0	260.2	264.4	268.6	272.8	277.0	281.2	285.4	291.3	296.3	304.7	313.1	321.5	329.9
	$T_{1\rho}$ [ms]	29.0	22.6	18.0	15.7	11.2	11.2	8.6	9.5	8.8	9.1	6.8	9.1	9.2	10.4	12.4	15.0	21.0	25.0
	k [10^5 s^{-1}]	1.14	1.48	1.91	2.23	3.45	3.45	5.88	4.56	5.46	5.01	10.5	12.3	12.6	15.9	20.6	26.2	38.4	46.3

[a]) Signal at 122 ppm. [b]) Signal at 44 ppm.

time, 1 ms; relaxation delay, 5 s; acquisition time, 100 ms, 4 K data points, 512 transients; total exper. time *ca.* 1 h. For the temp.-dependent spectra, we used the *Bruker BVT-2000* unit after calibration with phase transitions for the compounds adamantane, D-camphor, pivalic acid, and 1,4-diazabicyclooctane [26]. For the $T_{1\rho}$ measurements, the CP pulse sequence was complemented before signal detection by a variable delay time τ and the SELTICS sequence [15] for the suppression of side bands. The relevant data for the line shape and $T_{1\rho}$ experiments are collected in *Table 4*, and the measured rate constants are in *Tables 2* and *5*. The softwares used for spectral simulation were the programs MEXICO for the line-shape calculations [27] and MXET1 for the simulation of the ^{2}H spectra [28].

REFERENCES

[1] S. Jost, M. Kühnen, H. Günther, *Magn. Reson. Chem.* **2006**, *44*, 909.

[2] a) J. Grutzner, 'Encyclopedia of NMR', Eds. D. M. Grant, R. K. Harris, Wiley, Chichester, 2002, Vol. 9, p. 481; b) H. Günther, 'Encyclopedia of NMR', Eds. D. M. Grant, R. K. Harris, Wiley, Chichester, 1996; p. 2807; c) H. Günther, 'High-resolution 6/7Li NMR of Organolithium Compounds', in 'Advanced Applications of NMR to Organometallic Chemistry', Eds. M. Gielen, R. Willem, B. Wrackmeyer, Wiley, Chichester, 1996.

[3] a) T. Stey, D. Stalke, 'The Chemistry of Organolithium Compounds', Part 1, Eds. Z. Rappoport, I. Marek, pp. 47–120, Wiley, Chichester, 2004; b) E. Weiss, *Angew. Chem.* **1993**, *105*, 1565; *Angew. Chem., Int. Ed.* **1993**, *32*, 1501; c) K. Gregory, P. v. R. Schleyer, R. Snaith, *Adv. Inorg. Chem.* **1991**, *37*, 47; d) W. N. Setzer, R. v. R. Schleyer, *Adv. Organomet. Chem.* **1985**, *24*, 353.

[4] G. Fraenkel, H. Liu, *J. Am. Chem. Soc.* **2004**, *126*, 5202, and refs. cit. therein.

[5] a) J. Cabral, G. Fraenkel, *J. Am. Chem. Soc.* **1992**, *114*, 9067; b) G. Boche, G. Fraenkel, J. Cabral, K. Harms, N. J. R. van Eikema Hommes, J. Lohrenz, M. Marsch, P. v. R. Schleyer, *J. Am. Chem. Soc.* **1992**, *114*, 1562.

[6] D. Johnels, H. Günther, 'The Chemistry of Organolithium Compounds', Part 1, Eds. Z. Rappoport, I. Marek, pp. 47–120, Wiley, Chichester, 2004.

[7] W. Domalewski, F. G. Riddell, L. Stefaniak, *Bull. Pol. Acad. Sci., Chem.* **1998**, *46*, 35.

[8] W. Baumann, Y. Oprunenko, H. Günther, *Z. Naturforsch., A* **1995**, *50*, 429.

[9] a) J. Sandström, 'Dynamic NMR Spectroscopy', Academic Press, London, 1982; b) J. Kaplan, G. Fraenkel, 'NMR of Chemically Exchanging Systems', Academic Press, 1980.

[10] a) F. G. Riddell, 'Encyclopedia of NMR', Eds. D. M. Grant, R. K. Harris, Wiley, Chichester, 1996, Vol. 9, p. 570; b) F. G. Riddell, S. Arumugam, K. D. M. Harris, M. Rogerson, J. H. Strange, *J. Am. Chem. Soc.* **1993**, *115*, 1881.

[11] R. Zerger, W. Rhine, G. D. Stucky, *J. Am. Chem. Soc.* **1974**, *96*, 5441.

[12] P.-O. Quist, H. Förster, D. Johnels, *J. Am. Chem. Soc.* **1997**, *119*, 5390.

[13] D. Johnels, A. Anderson, A. Boman, U. Edlund, *Magn. Reson. Chem.* **1996**, *34*, 908.

[14] M. Kühnen, H. Günther, J.-P. Amoureux, C. Fernandéz, *Magn. Reson. Chem.* **2002**, *40*, 24.

[15] J. Hong, G. S. Harbison, *J. Magn. Reson., Ser. A* **1993**, *105*, 128.

[16] W. P. Rothwell, J. S. Waugh, *J. Chem. Phys.* **1981**, *74*, 2721.

[17] D. Johnels, U. Edlund, *J. Am. Chem. Soc.* **1990**, *112*, 1647.

[18] H. S. Gutowsky, C. H. Holm, *J. Chem. Phys.* **1956**, *25*, 1228.

[19] H. Günther, 'NMR Spectroscopy', Wiley, Chichester, 1995.

[20] G. Fraenkel, J. Cabral, C. Lanter, J. Wang, *J. Org. Chem.* **1999**, *64*, 1302.

[21] M. J. Duer, 'Solid-State NMR Spectroscopy', Blackwell Science, Oxford, 2002.

[22] C. A. Fyfe, 'Solid State NMR for Chemists', C. F. C. Press, Guelph, Ontario, 1983.

[23] N. Moazzen-Ahmadi, H. P. Gush, M. Halpern, H. Jagannath, A. Leung, I. Ozier, *J. Chem. Phys.* **1987**, *88*, 563.

[24] T. Nishikawa, *J. Phys. Soc. Jpn.* **1957**, *12*, 668; T. Itoh, *J. Phys. Soc. Jpn.* **1956**, *11*, 264.

[25] F. G. Riddell, M. Rogerson, *Magn. Reson. Chem.* **1997**, *35*, 333.

[26] F. G. Riddell, R. A. Spark, G. V. Günther, *Magn. Reson. Chem.* **1996**, *34*, 824; J. F. Haw, R. A. Cook, R. C. Crosby, *J. Magn. Reson.* **1986**, *66*, 551.

[27] A. D. Bain, D. M. Rex, R. N. Smith, *Magn. Reson. Chem*. **2001**, *39*, 122.
[28] M. S. Greenfield, A. D. Ronemus, R. L. Vold, R. R. Vold, P. D. Ellis, T. E. Raidy, *J. Magn. Reson*. **1987**, *72*, 89, and private communication by R. R. Vold.

Received August 15, 2012